# Negligible Environmental Sensitivity of Graphene in a Hexagonal Boron Nitride/Graphene/h-BN Sandwich Structure

**Lei Wang,[†,∥] Zheyuan Chen,[‡,∥] Cory R. Dean,[†,§] Takashi Taniguchi,[⊥] Kenji Watanabe,[⊥] Louis E. Brus,[‡,*] and James Hone[†,*]**

[†]Department of Mechanical Engineering, [‡]Department of Chemistry and [§]Electrical Engineering, Columbia University, New York, New York 10027, United States and [⊥]Advanced Materials Laboratory, National Institute for Materials Science, 1-1 Namiki, Tsukuba 305-0044, Japan. [∥]These authors contributed equally to this work.

**ABSTRACT** Using Raman spectroscopy, we study the environmental sensitivity of mechanically exfoliated and electrically floating single-layer graphene transferred onto a hexagonal boron nitride (h-BN) substrate, in comparison with graphene deposited on a $SiO_2$ substrate. In order to understand and isolate the substrate effect on graphene electrical properties, we model and correct for Raman optical interference in the substrates. As-deposited and unannealed graphene shows a large $I_{2D}/I_G$ ratio on both substrates, indicating extremely high quality, close to that of graphene suspended in vacuum. Thermal annealing strongly activates subsequent environmental sensitivity on the $SiO_2$ substrate; such activation is reduced but not eliminated on the h-BN substrate. In contrast, in a h-BN/graphene/h-BN sandwich structure, with graphene protected on both sides, graphene remains pristine despite thermal processing. Raman data provide a deeper understanding of the previously observed improved graphene electrical conductivity on h-BN substrates. In the sandwich structure, the graphene 2D Raman feature has a higher frequency and narrower line width than in pristine suspended graphene, implying that the local h-BN environment modestly yet measurably changes graphene electron and phonon dispersions.

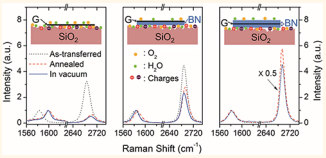


**KEYWORDS:** graphene · hexagonal boron nitride · Raman · heterostructure · layer materials

Single-layer graphene supported on a $SiO_2$ substrate has an electronic mobility[1,2] far below the theoretical prediction. The mobility of graphene suspended in vacuum is actually 10 times higher than that of $SiO_2$ supported devices. It is now understood that the graphene electrical properties are strongly perturbed by the surface roughness,[3−5] interfacial charged impurities,[6,7] and surface phonons of $SiO_2$ substrates.[6,8] Thus graphene devices built upon a $SiO_2$ substrate typically have compromised properties. Atomically flat hexagonal boron nitride (h-BN), with a large band gap and similar lattice constant as graphene, is a far better substrate.[9] The mobility for graphene devices on h-BN was observed to be 1 order of magnitude better than devices on $SiO_2$, promising an emerging age of high-quality graphene devices.

Graphene, with every atom on the surface, shows a molecule-like sensitivity to its surroundings. It is important to understand and control this environmental sensitivity. Confocal Raman spectroscopy is a sensitive noncontact tool which provides precise information on graphene lattice strain, structural defects, electrical doping, and electron scattering, without the necessity of processing to make electrical contacts.[10−15] In this article, we present the first Raman study of graphene on a h-BN substrate. Our data, together with the prior electrical characterization, provide a deeper understanding of environmental effects on graphene on both $SiO_2$ and h-BN substrates.

## RESULTS AND DISCUSSION

The optical images of two types of graphene samples are presented in Figure 1, with detailed information given in the Experimental Section. Figure 2 shows the Raman spectra of G and 2D peaks for the both types of samples under three different conditions. The black dotted lines are obtained on the as-transferred samples under ambient conditions. The red dashed lines are taken on the same samples after annealing, and the Raman mapping is still carried out under ambient conditions. The blue solid lines are taken on the same annealed samples but in a vacuum chamber. The absence of a D peak (see Figure S6 of Supporting Information) suggests that the thermal annealing used in our experiment does not

* Address correspondence to leb26@columbia.edu, jh2228@columbia.edu.

Received for review August 30, 2012 and accepted September 25, 2012.

**Published online September 25, 2012**
10.1021/nn304004s

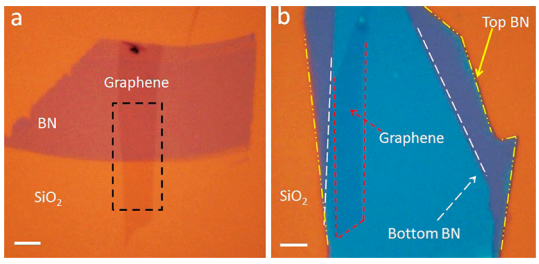


**Figure 1. Two types of samples under study (a) Optical image of a type I sample, a single-layer graphene flake transferred partially onto a 5.7 nm thick h-BN flake and partially on a $SiO_2$ substrate. Raman mapping is carried out in the region inside the dashed rectangle. (b) Optical image of a type II sample, a single graphene flake encapsulated between two h-BN flakes. The scale bars in both images are 5 $\mu$m in length.**

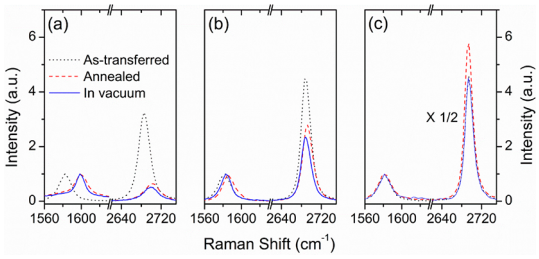


**Figure 2. Observed Raman spectra of as-transferred (black dotted lines), annealed (red dashed lines) graphene, and annealed graphene subsequently observed in vacuum (blue solid lines) on $SiO_2$/Si (a), on h-BN (b), and between two h-BN layers (c). Each spectrum was normalized according to its G peak. The intensity of both 2D peaks in (c) was multiplied by a factor of 1/2 for comparison. The interference effect is not removed.**

introduce detectable level of defects. The analysis of the correlation[16,17] between the position of the 2D peak ($\omega_{2D}$) and the G peak ($\omega_G$) indicates that the strain plays a negligible role during annealing (see Figure S7 of Supporting Information).

Let us first focus on the type I samples. For as-transferred graphene on $SiO_2$ and on h-BN, their G peaks have similar positions and widths. The G peak position and width depend strongly on the interaction between graphene and its environment. Any charge transfer between graphene and the environment leads to a stiffened (upshifted) and narrowed G peak.[12,13] The stiffening stems from the reduction of strong electron−lattice vibration coupling as the Fermi level shifts, while the narrowed peak is the result of a longer phonon lifetime as decay into electron−hole pairs is blocked.[12,13] The previous studies of graphene on $SiO_2$[12,13] and suspended graphene[18,19] showed that G peak position of the pristine graphene is close to 1581 $cm^{-1}$. In Figure 3 (top), the initial G peak shows a similar position $\omega_G$ (1581−1582 $cm^{-1}$) and width $\Gamma_G$ (11−12 $cm^{-1}$) on both substrates. These values are essentially consistent with those of pristine graphene, indicating that as-transferred graphene is negligibly doped, at or below a level of $\sim 1 \times 10^{12}$ $cm^{-2}$.[18]

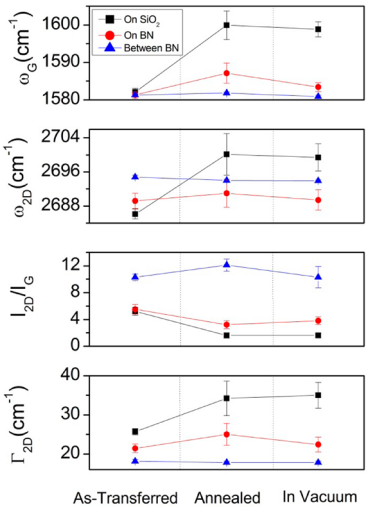


**Figure 3. Environmental sensitivity of graphene Raman data on $SiO_2$/Si (black square), on h-BN (red circle), and between two h-BN layers (blue triangle). Each dot represents the average value determined from Raman mapping shown in Supporting Information. The corresponding experimental uncertainties were estimated from the standard deviation in Raman mapping. The interference effect is removed in $I_{2D}/I_G$.**

Figure 3 (bottom) shows the comparison of the 2D peak width ($\Gamma_{2D}$). The $\Gamma_{2D}$ of the graphene on the $SiO_2$ part is between 25 and 26 $cm^{-1}$, which agrees with previous reported values.[10,19] For the section of graphene on h-BN, the $\Gamma_{2D}$ is between 22 and 23 $cm^{-1}$, decreasing by $\sim$4 $cm^{-1}$ compared with the value of graphene on $SiO_2$. The peak shape and the amount of decrease in $\Gamma_{2D}$ are similar to that observed on the suspended graphene samples.[17,18] The 2D peak position $\omega_{2D}$ is also slightly different on the two substrates: The 2D peak upshifts by $\sim$3 $cm^{-1}$ for graphene on h-BN, from 2686 $cm^{-1}$ for graphene on $SiO_2$. The increase in $\omega_{2D}$ of graphene on h-BN here, however, is different from the behavior of the suspended graphene.[17,20] On h-BN, we have repeatedly observed an upshifted 2D peak centered near 2689 $cm^{-1}$ when excited by 514.5 nm laser, while it is downshifted to $\sim$2674 $cm^{-1}$ for suspended graphene.[20] This upshift is discussed below in the section describing results for the h-BN sandwich structure.

The integrated intensity ratio $I_{2D}/I_G$ of the G and 2D peaks provides additional and independent information.[20,21] The intense 2D peak is doubly electronically resonant, and all electron scattering processes in the resonant intermediate states decrease its intensity.[22] In contrast, the G peak intensity is not affected by such scattering processes.[23] Thus, the highest $I_{2D}/I_G$ ratio occurs in perfectly pristine graphene. Environmental stray electrical fields, for example, from oxide impurity charges, can increase scattering. For this reason, an annealed graphene sample, conformal on a $SiO_2$ substrate, shows an $I_{2D}/I_G$ ratio much lower than for suspended graphene. In addition, scattering increases

with increased carrier concentration due to the Fermi level shift.[19] An electrochemical gating experiment shows that $I_{2D}/I_G$ decreases upon either electron or hole doping.[11] At very high hole doping, the ratio further diminishes,[24] in agreement with off-resonance electronic Raman enhancement theory imposed by the Pauli exclusion principle.[25] The $I_{2D}/I_G$ ratio also depends on laser polarization[26] and spectrometer sensitivity.[23,27]

In addition to these intrinsic intensity effects, there is an optical interference effect in the $SiO_2$ layer[28,29] which enhances the G peak intensity by a factor of ~2 on $SiO_2$/Si, compared with suspended graphene.[21] The near 40 nm difference in the G and 2D scattering wavelengths leads to different multiple reflection interference. Therefore, the observed $I_{2D}/I_G$ ratio systematically varies as a function of $SiO_2$ thickness and laser excitation frequency.[29] In our experiment, the additional h-BN layer between graphene and $SiO_2$ further complicates this interference.

We now calculate this optical interference effect on BN supported on $SiO_2$ to understand the intrinsic substrate effect on relative graphene Raman intensities. To calculate optical interference, we adopt the multi-reflection Fresnel model of the Raman scattering developed by Yoon *et al.*[29] There are four interfaces associated with our experiment: air/graphene, graphene/h-BN, h-BN/$SiO_2$, and $SiO_2$/Si. The effective reflection coefficient of adjacent interfaces is introduced to reduce the interface number and simplify the calculation, as described in the Supporting Information.[28]

The calculated interference enhancement factor *F* for $I_{2D}/I_G$ in Figure S1 in Supporting Information shows an oscillatory pattern as h-BN thickness increases from 0 to 500 nm. The factor *F* has a global maximum of 2.04 on 65 nm h-BN and a global minimum of 0.62 on 125 nm h-BN. An enhancement of $I_{2D}/I_G$ from its intrinsic value is observed for nearly three-quarters of h-BN thickness in the range from 0 to 500 nm. In our experiment, the observed $I_{2D}/I_G$ ratio of as-transferred graphene on h-BN is 6.3, which can be corrected using Figure S3 to 5.5 $I_{2D}/I_G$ on $SiO_2$. If the interference in the $SiO_2$ itself is removed, the ratios are 6 and 5.7 on the h-BN and oxide substrates.

The ratios for these as-transferred graphene on $SiO_2$ and on h-BN are nearly equal: ~6. This near equality was observed in four different samples: the observed value was higher in two samples, nearly ~10 in one sample. These high ratios are close to the reported high ratio measured for intrinsic suspended graphene.[20,21] These Raman data reveal the very high intrinsic quality of directly exfoliated graphene samples, observed without further processing (*e.g.*, annealing), necessary to make electrical connections on both oxide and h-BN.

Exfoliated as-transferred graphene on h-BN and $SiO_2$, in principle, can be contaminated by both PMMA and tape residue. The extent of such contamination varies from sample to sample and laboratory to laboratory, typically in an uncharacterized fashion. Thermal annealing in a reducing atmosphere has been used as a standard procedure to remove possible contamination, for example, before further characterization in STM studies[3,5] and electrical measurement.[9] Detailed study on the removal of PMMA through thermal annealing was carried out using Raman spectroscopy and transmission electron microscopy (TEM).[30] Careful studies have shown that annealing graphene exfoliated directly on a $SiO_2$/Si substrate creates better conformation to the somewhat rough oxide surface. The increased graphene distortion enables greater subsequent doping by oxygen and water under ambient conditions.[31,32] Initially, the directly exfoliated graphene sits on the high spots of the $SiO_2$/Si substrate and is less perturbed.[32] Thus, somewhat paradoxically, we find that annealing on oxide substrates actually creates less intrinsic graphene when subsequently observed under ambient conditions.

Now we describe the Raman mapping (taken in ambient conditions) after annealing in forming gas at 340 °C for 3 h. On both $SiO_2$ and h-BN substrates, there are substantial changes in the Raman data. The $I_{2D}/I_G$ ratio decreases by about 40% on h-BN and 70% on $SiO_2$/Si. This decrease is accompanied by the stiffening of G slightly to 1587 $cm^{-1}$ on h-BN and more substantially to 1600 $cm^{-1}$ on $SiO_2$/Si. As mentioned above, this behavior on $SiO_2$/Si has been previously observed. The position of 2D peak changes negligibly on h-BN, with only a 1 $cm^{-1}$ increase. The position upshifts by 15 to 2701 $cm^{-1}$ on $SiO_2$/Si. This upshift suggests hole doping,[11] consistent with earlier reports on $SiO_2$/Si supported graphene.[31−33] Even though annealing broadens 2D peaks on both substrates, annealed graphene on h-BN still possesses a quite narrow 2D peak (only 25 $cm^{-1}$ in width), close to that of as-transferred graphene. If we use the calibration from a recent electrochemical top gating Raman study,[11] then exposing our annealed graphene in air makes it hole doped at $\sim 1.5 \times 10^{12}$ $cm^{-2}$ on h-BN and $\sim 1.3 \times 10^{13}$ $cm^{-2}$ on $SiO_2$/Si. The presence of h-BN substrate suppresses ~88% of doping on $SiO_2$/Si upon annealing. This strong suppression is consistent with the observation of superb electronic transport properties of the graphene device on h-BN.[9]

To understand the role of ambient oxygen and moisture, we further took annealed graphene Raman data in a vacuum chamber pumped down to $1 \times 10^{-5}$ Torr, as described above. The spectra of graphene on $SiO_2$/Si do not change noticeably, except for a 2 $cm^{-1}$ downshift in the G peak position. This downshift represents a slight doping decrease of $1 \times 10^{12}$ $cm^{-2}$, but graphene was still strongly doped at $1.2 \times 10^{13}$ $cm^{-2}$ on $SiO_2$/Si. For graphene on h-BN, the G peak downshifts to 1583.5 $cm^{-1}$, close to pristine value. The downshift is also companied by 20% increase in

$I_{2D}/I_G$ ratio and 2D peak narrowing by 2 $cm^{-1}$. Those changes suggest more pristine-like graphene on h-BN when annealed graphene was placed in vacuum. If this sample is removed from vacuum and again studied in ambient, the Raman G peak on h-BN shifts back to the original position as before placed in the vacuum. Thus, on h-BN, the ambient doping effect is largely reversible.

The observed doping of annealed graphene on h-BN in ambient can be attributed to a modest reversible binding of oxygen and water to "distorted" graphene on h-BN, activated by thermal annealing. Two types of mechanisms were introduced to analyze the doping of supported graphene by the local environment: (1) direct charge transfer between graphene and adsorbates of different electronegativity, and (2) redox reactions of graphene with water and adsorbates.[34] The electrochemical mechanism has been used to explain the different doping behaviors by ammonium (n-type) and humid atmospheres (p-type).[34,35] In prior work, the combination of Raman spectroscopy and scanning tunneling microscopy suggests that the hole doping to graphene on $SiO_2$/Si substrates comes from the interaction with $O_2$ bound to the silicon dioxide surface and is facilitated in the presence of water.[31,32] As mentioned above, the exfoliated graphene originally sits on the high spots of the $SiO_2$/Si substrate.[32] After annealing, graphene is brought to be in close contact with the $SiO_2$/Si substrate and conforms to the surface roughness, resulting in a distorted graphene that is closer to oxide electric fields. When close enough, charge or impurities in $SiO_2$/Si reaches an equilibrium of charge transfer with graphene, while distortion increases binding of oxygen or water to graphene and dopes graphene through an electrochemical mechanism. For graphene on h-BN, the chemically inert nature of the substrate, such as the absence of dangling bonds and charge impurities, introduces a negligible amount of disorder to graphene, as reported in previous STM studies.[36,37] A strong van der Waals interaction exists at the interface between the two layers; in fact, h-BN can be used as a metal-free substrate to grow graphene through the chemical vapor deposition (CVD) method.[38,39] This strong interaction may block the intrusion of gas molecules into the graphene−substrate interface, which is usually present in the conventional Si/$SiO_2$ substrate.

There is some sample-to-sample variation. For most graphene on h-BN samples, annealing upshifts the G peak to the range of 1587−1592 $cm^{-1}$: in about 10% of samples, the G peak remained unchanged on h-BN, while graphene on $SiO_2$/Si was doped to the similar level described previously on $SiO_2$/Si.

Furthermore, we also noticed that the mechanically exfoliated h-BN exhibited irregular fluorescence background, independent of thermal annealing and varying from spot to spot. Since h-BN is a deep-UV light emitter,[40] the fluorescence background could be due to the impurity states introduced during synthesis. Because the similar background shows up in both graphene-covered and uncovered region, we suggest that the impurity is embedded inside h-BN, not just on the surface. Due to the strong optical absorption of graphene (in terms of one-atom-thick material), the fluorescence would be efficiently quenched if graphene is in close contact with the emission center.[41] This strong background observed can interfere with the G peak; therefore, such samples were discarded in our study.

Thus we see that the Raman electronic properties of graphene supported on the BN substrate, while superior to those on $SiO_2$, are degraded somewhat due to exposing to air after thermal annealing. Would this occur if graphene was protected by BN on both sides rather than one side? We did Raman mapping on as-transferred and annealed graphene in the h-BN/graphene/h-BN sandwich structure, in ambient and in vacuum as described above. The graphene Raman data (Figures S11−S13, Supporting Information) show that the quality of graphene encapsulated by BN on both side remains as good as the best pristine graphene. As shown in Figure 2 and Figure 3, the position and width of the G peak are 1581 and 16 $cm^{-1}$, respectively, indicating that the doping level is smaller than the Raman detection limit. In contrast to single-sided support on h-BN, the Raman data remain unchanged after thermal annealing. The (interference corrected) $I_{2D}/I_G$ ratio is high, ~11, comparable to that of suspended graphene.[20,21] The 2D peak is further narrowed to 18 $cm^{-1}$ and stiffened to 2695 $cm^{-1}$, compared to that of one-sided h-BN supported graphene. In the sandwich structure, the width of overtone peak, 2D peak, is close to that of the G peak (16 $cm^{-1}$).

The doubly enhanced, very strong, two-phonon 2D Raman feature is composed of a range of phonon momentum along the K to Γ direction in the Brillouin zone. Recent calculation shows that the position and relatively narrow 2D width for pristine graphene represents the interplay of opposite trigonal warpings in electron and phonon dispersions.[42] We see that the 2D peak position systematically upshifts in the one-sided and sandwich h-BN structures. In the sandwich structure, the 2D feature peak is upshifted by 21 $cm^{-1}$, and the width decreased by 4−5 $cm^{-1}$, compared with suspended pristine graphene. Thus, the trigonal warping phonon and electron dispersions are changed somewhat in the h-BN sandwich structure compared with pristine graphene in vacuum. This likely represents the effect of the local BN dielectric constant on the intrinsic graphene electronic structure.

Annealing in a reducing hydrogen gas at high temperature has a negligible effect on graphene in the sandwich structure. Apparently, the strong van der Waals interaction between graphene and h-BN isolates

both sides of graphene from gas impurities (such as $O_2$ and $H_2O$) after high-temperature annealing processing. Although the impurity charge density level is reduced by 1 order of magnitude for graphene with one-sided support on h-BN, we still observe slight doping after thermal annealing, as a result of the equilibrium binding of gas molecules with the top side. The h-BN/graphene/h-BN sandwich offers great advantage in creating a stable, robust, near intrinsic graphene structure able to withstand thermal annealing procedures.

## CONCLUSION

In summary, the Raman data reveal a high initial quality and minor environmental perturbation for exfoliated graphene on both $SiO_2$ and h-BN substrates under ambient conditions if the sample has not been thermally annealed or processed. The observed high Raman $I_{2D}/I_G$ ratio and large G peak width for graphene on h-BN is similar to suspended graphene over a trench. On $SiO_2$, subsequent thermal annealing strongly activates graphene sensitivity to environmental doping by oxygen, water vapor, and charge impurities on the substrate. On the h-BN substrate, such thermal activation of environmental doping is reduced by 1 order of magnitude and varies slightly from sample to sample. This residual doping after annealing is apparently caused by weak, reversible binding of oxygen and water and is further reduced by pumping in vacuum. An essentially complete removal of environmental influence is achieved for graphene in a h-BN/graphene/h-BN sandwich. The encapsulation of graphene on both sides is required to keep graphene unperturbed during high-temperature processing in a reducing atmosphere. In addition, the h-BN local environment in the sandwich structure produces the highest graphene 2D Raman peak position and the narrowest width yet observed. Our study supports the suitability of h-BN substrates, especially the sandwich structure, for high-quality graphene devices.

## EXPERIMENTAL SECTION

Two types of samples were made to study the environmental effects on graphene devices. The first type of sample is used to compare graphene on $SiO_2$ and h-BN substrates. As shown in Figure 1a, the h-BN flakes were first deposited on the 285 nm $SiO_2$ on the Si substrate by the mechanical exfoliation method. Then a single-layer graphene flake was transferred onto a h-BN flake using the techniques described in our previous work.[9] Immediately after transfer, Raman spectroscopy was first carried out to inspect the single-layer graphene flakes which are partially on h-BN and partially on $SiO_2$ substrates. The measurements were performed in ambient at 25 °C. As-transferred graphene on BN samples was then annealed with forming gas ($H_2$/Ar) in quartz tubing placed inside a furnace at 340 °C for 3 h. After thermal annealing, Raman spectra were first taken in ambient condition. Then the sample was mounted inside a vacuum chamber with an optical window which was pumped down to $1 \times 10^{-5}$ Torr by a diffusion pump. The Raman spectra of the sample in vacuum were obtained at room temperature.

The second type of the sample was made to further investigate the graphene devices encapsulated by h-BN on both sides. As shown in Figure 1b, a single-layer graphene was sandwiched between bottom and top h-BN flakes. Raman spectroscopy was then carried out in the same condition as type I samples. The Raman mapping of the type I sample as-transferred, annealed, and in vacuum is shown in Supporting Information Figures S8, S9, and S10, respectively. The Raman mapping of the type II sample as-transferred, annealed, and in vacuum is shown in Supporting Information Figures S11, S12, and S13 respectively. The average values of every Raman feature for both types of samples are plotted in Figures 2 and 3.

To make sure that contamination does not play a role in our Raman study, we examined the surfaces of graphene and h-BN using AFM after mechanical exfoliation and each transfer process step. Any sample with noticeable contamination observed in AFM images was discarded immediately. In this way, the pristine properties of graphene are preserved in the h-BN/graphene/h-BN sandwich structure through each step and annealing process.

*Conflict of Interest:* The authors declare no competing financial interest.

*Acknowledgment.* We thank D. M. Basco of CNRS for informative correspondence on graphene Raman theory, and S. Ryu, P. Kim, and T.F. Heinz for inspiring discussions. This work was supported by National Science Foundation through the MIRT program (Grant No. DMR-1122594).

*Supporting Information Available:* Interference effect calculation based on multiple-reflection model, Raman maps, and the correlation of G and 2D peak positions of graphene supported on different substrates. This material is available free of charge *via* the Internet at http://pubs.acs.org.

## REFERENCES AND NOTES

1. Castro Neto, A. H.; Guinea, F.; Peres, N. M. R.; Novoselov, K. S.; Geim, A. K. The Electronic Properties of Graphene. *Rev. Mod. Phys.* **2009**, *81*, 109–162.
2. Geim, A. K.; Novoselov, K. S. The Rise of Graphene. *Nat. Mater.* **2007**, *6*, 183–191.
3. Ishigami, M.; Chen, J. H.; Cullen, W. G.; Fuhrer, M. S.; Williams, E. D. Atomic Structure of Graphene on $SiO_2$. *Nano Lett.* **2007**, *7*, 1643–1648.
4. Morozov, S. V.; Novoselov, K. S.; Katsnelson, M. I.; Schedin, F.; Elias, D. C.; Jaszczak, J. A.; Geim, A. K. Giant Intrinsic Carrier Mobilities in Graphene and Its Bilayer. *Phys. Rev. Lett.* **2008**, *100*, 016602.
5. Stolyarova, E.; Rim, K. T.; Ryu, S. M.; Maultzsch, J.; Kim, P.; Brus, L. E.; Heinz, T. F.; Hybertsen, M. S.; Flynn, G. W. High-Resolution Scanning Tunneling Microscopy Imaging of Mesoscopic Graphene Sheets on an Insulating Surface. *Proc. Natl. Acad. Sci. U.S.A.* **2007**, *104*, 9209–9212.
6. Chen, J. H.; Jang, C.; Xiao, S. D.; Ishigami, M.; Fuhrer, M. S. Intrinsic and Extrinsic Performance Limits of Graphene Devices on $SiO_2$. *Nat. Nanotechnol.* **2008**, *3*, 206–209.
7. Hwang, E. H.; Adam, S.; Das Sarma, S. Carrier Transport in Two-Dimensional Graphene Layers. *Phys. Rev. Lett.* **2007**, *98*, 186806.
8. Fratini, S.; Guinea, F. Substrate-Limited Electron Dynamics in Graphene. *Phys. Rev. B* **2008**, *77*, 195415.
9. Dean, C. R.; Young, A. F.; Meric, I.; Lee, C.; Wang, L.; Sorgenfrei, S.; Watanabe, K.; Taniguchi, T.; Kim, P.; Shepard, K. L.; *et al.* Boron Nitride Substrates for High-Quality Graphene Electronics. *Nat. Nanotechnol.* **2010**, *5*, 722–726.
10. Ferrari, A. C.; Meyer, J. C.; Scardaci, V.; Casiraghi, C.; Lazzeri, M.; Mauri, F.; Piscanec, S.; Jiang, D.; Novoselov, K. S.; Roth, S.; *et al.* Raman Spectrum of Graphene and Graphene Layers. *Phys. Rev. Lett.* **2006**, *97*, 187401.

11. Das, A.; Pisana, S.; Chakraborty, B.; Piscanec, S.; Saha, S. K.; Waghmare, U. V.; Novoselov, K. S.; Krishnamurthy, H. R.; Geim, A. K.; Ferrari, A. C.; *et al.* Monitoring Dopants by Raman Scattering in an Electrochemically Top-Gated Graphene Transistor. *Nat. Nanotechnol.* **2008**, *3*, 210–215.
12. Pisana, S.; Lazzeri, M.; Casiraghi, C.; Novoselov, K. S.; Geim, A. K.; Ferrari, A. C.; Mauri, F. Breakdown of the Adiabatic Born–Oppenheimer Approximation in Graphene. *Nat. Mater.* **2007**, *6*, 198–201.
13. Yan, J.; Zhang, Y. B.; Kim, P.; Pinczuk, A. Electric Field Effect Tuning of Electron–Phonon Coupling in Graphene. *Phys. Rev. Lett.* **2007**, *98*, 166802.
14. Huang, M. Y.; Yan, H. G.; Chen, C. Y.; Song, D. H.; Heinz, T. F.; Hone, J. Phonon Softening and Crystallographic Orientation of Strained Graphene Studied by Raman Spectroscopy. *Proc. Natl. Acad. Sci. U.S.A.* **2009**, *106*, 7304–7308.
15. Mohiuddin, T. M. G.; Lombardo, A.; Nair, R. R.; Bonetti, A.; Savini, G.; Jalil, R.; Bonini, N.; Basko, D. M.; Galiotis, C.; Marzari, N.; *et al.* Uniaxial Strain in Graphene by Raman Spectroscopy: G Peak Splitting, Gruneisen Parameters, and Sample Orientation. *Phys. Rev. B* **2009**, *79*, 205433.
16. Shim, J.; Lui, C. H.; Ko, T. Y.; Yu, Y. J.; Kim, P.; Heinz, T. F.; Ryu, S. Water-Gated Charge Doping of Graphene Induced by Mica Substrates. *Nano Lett.* **2012**, *12*, 648–654.
17. Gong, C.; Hinojos, D.; Wang, W. C.; Nijem, N.; Shan, B.; Wallace, R. M.; Cho, K. J.; Chabal, Y. J. Metal–Graphene–Metal Sandwich Contacts for Enhanced Interface Bonding and Work Function Control. *ACS Nano* **2012**, *6*, 5381–5387.
18. Lazzeri, M.; Mauri, F. Nonadiabatic Kohn Anomaly in a Doped Graphene Monolayer. *Phys. Rev. Lett.* **2006**, *97*, 266407.
19. Casiraghi, C.; Pisana, S.; Novoselov, K. S.; Geim, A. K.; Ferrari, A. C. Raman Fingerprint of Charged Impurities in Graphene. *Appl. Phys. Lett.* **2007**, *91*, 233108.
20. Berciaud, S.; Ryu, S.; Brus, L. E.; Heinz, T. F. Probing the Intrinsic Properties of Exfoliated Graphene: Raman Spectroscopy of Free-Standing Monolayers. *Nano Lett.* **2009**, *9*, 346–352.
21. Ni, Z. H.; Yu, T.; Luo, Z. Q.; Wang, Y. Y.; Liu, L.; Wong, C. P.; Miao, J. M.; Huang, W.; Shen, Z. X. Probing Charged Impurities in Suspended Graphene Using Raman Spectroscopy. *ACS Nano* **2009**, *3*, 569–574.
22. Basko, D. M.; Piscanec, S.; Ferrari, A. C. Electron–Electron Interactions and Doping Dependence of the Two-Phonon Raman Intensity in Graphene. *Phys. Rev. B* **2009**, *80*, 165413.
23. Casiraghi, C. Doping Dependence of the Raman Peaks Intensity of Graphene Close to the Dirac Point. *Phys. Rev. B* **2009**, *80*, 233407.
24. Jung, N.; Kim, N.; Jockusch, S.; Turro, N. J.; Kim, P.; Brus, L. Charge Transfer Chemical Doping of Few Layer Graphenes: Charge Distribution and Band Gap Formation. *Nano Lett.* **2009**, *9*, 4133–4137.
25. Chen, C. F.; Park, C. H.; Boudouris, B. W.; Horng, J.; Geng, B. S.; Girit, C.; Zettl, A.; Crommie, M. F.; Segalman, R. A.; Louie, S. G. Controlling Inelastic Light Scattering Quantum Pathways in Graphene. *Nature* **2011**, *471*, 617–620.
26. Yoon, D.; Moon, H.; Son, Y. W.; Samsonidze, G.; Park, B. H.; Kim, J. B.; Lee, Y.; Cheong, H. Strong Polarization Dependence of Double-Resonant Raman Intensities in Graphene. *Nano Lett.* **2008**, *8*, 4270–4274.
27. Casiraghi, C. Raman Intensity of Graphene. *Phys. Status Solidi B* **2011**, *248*, 2593–2597.
28. Wang, Y. Y.; Ni, Z. H.; Shen, Z. X.; Wang, H. M.; Wu, Y. H. Interference Enhancement of Raman Signal of Graphene. *Appl. Phys. Lett.* **2008**, *92*, 043121.
29. Yoon, D.; Moon, H.; Son, Y. W.; Choi, J. S.; Park, B. H.; Cha, Y. H.; Kim, Y. D.; Cheong, H. Interference Effect on Raman Spectrum of Graphene on $SiO_2$/Si. *Phys. Rev. B* **2009**, *80*, 125422.
30. Lin, Y. C.; Lu, C. C.; Yeh, C. H.; Jin, C. H.; Suenaga, K.; Chiu, P. W. Graphene Annealing: How Clean Can It Be?. *Nano Lett.* **2012**, *12*, 414–419.
31. Liu, L.; Ryu, S. M.; Tomasik, M. R.; Stolyarova, E.; Jung, N.; Hybertsen, M. S.; Steigerwald, M. L.; Brus, L. E.; Flynn, G. W. Graphene Oxidation: Thickness-Dependent Etching and Strong Chemical Doping. *Nano Lett.* **2008**, *8*, 1965–1970.
32. Ryu, S.; Liu, L.; Berciaud, S.; Yu, Y. J.; Liu, H. T.; Kim, P.; Flynn, G. W.; Brus, L. E. Atmospheric Oxygen Binding and Hole Doping in Deformed Graphene on a $SiO_2$ Substrate. *Nano Lett.* **2010**, *10*, 4944–4951.
33. Pirkle, A.; Chan, J.; Venugopal, A.; Hinojos, D.; Magnuson, C. W.; McDonnell, S.; Colombo, L.; Vogel, E. M.; Ruoff, R. S.; Wallace, R. M. The Effect of Chemical Residues on the Physical and Electrical Properties of Chemical Vapor Deposited Graphene Transferred to $SiO_2$. *Appl. Phys. Lett.* **2011**, *99*, 122108.
34. Pinto, H.; Jones, R.; Goss, J. P.; Briddon, P. R. Mechanisms of Doping Graphene. *Phys. Status Solidi A* **2010**, *207*, 2131–2136.
35. Schedin, F.; Geim, A. K.; Morozov, S. V.; Hill, E. W.; Blake, P.; Katsnelson, M. I.; Novoselov, K. S. Detection of Individual Gas Molecules Adsorbed on Graphene. *Nat. Mater.* **2007**, *6*, 652–655.
36. Decker, R.; Wang, Y.; Brar, V. W.; Regan, W.; Tsai, H. Z.; Wu, Q.; Gannett, W.; Zettl, A.; Crommie, M. F. Local Electronic Properties of Graphene on a Bn Substrate *via* Scanning Tunneling Microscopy. *Nano Lett.* **2011**, *11*, 2291–2295.
37. Xue, J. M.; Sanchez-Yamagishi, J.; Bulmash, D.; Jacquod, P.; Deshpande, A.; Watanabe, K.; Taniguchi, T.; Jarillo-Herrero, P.; Leroy, B. J. Scanning Tunnelling Microscopy and Spectroscopy of Ultra-flat Graphene on Hexagonal Boron Nitride. *Nat. Mater.* **2011**, *10*, 282–285.
38. Ding, X. L.; Ding, G. Q.; Xie, X. M.; Huang, F. Q.; Jiang, M. H. Direct Growth of Few Layer Graphene on Hexagonal Boron Nitride by Chemical Vapor Deposition. *Carbon* **2011**, *49*, 2522–2525.
39. Son, M.; Lim, H.; Hong, M.; Choi, H. C. Direct Growth of Graphene Pad on Exfoliated Hexagonal Boron Nitride Surface. *Nanoscale* **2011**, *3*, 3089–3093.
40. Kubota, Y.; Watanabe, K.; Tsuda, O.; Taniguchi, T. Deep Ultraviolet Light-Emitting Hexagonal Boron Nitride Synthesized at Atmospheric Pressure. *Science* **2007**, *317*, 932–934.
41. Chen, Z. Y.; Berciaud, S.; Nuckolls, C.; Heinz, T. F.; Brus, L. E. Energy Transfer from Individual Semiconductor Nanocrystals to Graphene. *ACS Nano* **2010**, *4*, 2964–2968.
42. Venezuela, P.; Lazzeri, M.; Mauri, F. Theory of Double-Resonant Raman Spectra in Graphene: Intensity and Line Shape of Defect-Induced and Two-Phonon Bands. *Phys. Rev. B* **2011**, *84*, 035433.